THE JOURNAL OF PHYSICAL CHEMISTRY Letters

Letter

pubs.acs.org/JPCL

Electrostatic Interaction-Induced Room-Temperature Phosphorescence in Pure Organic Molecules from QM/MM Calculations

Huili Ma,[†] Wen Shi,[†] Jiajun Ren,[†] Wenqiang Li,[†] Qian Peng,*[,‡] and Zhigang Shuai*[,†]

[†]Key Laboratory of Organic OptoElectronics and Molecular Engineering, Department of Chemistry, Tsinghua University, Beijing 100084, People's Republic of China

[‡]Key Laboratory of Organic Solids, Beijing National Laboratory for Molecular Science (BNLMS), Institute of Chemistry, Chinese Academy of Sciences, Beijing 100190, People's Republic of China

Supporting Information

ABSTRACT: Room temperature phosphorescence (RTP) from pure organic material is rare due to the low phosphorescence quantum efficiency. That is why the recent discovery of crystallization induced RTP for several organic molecules aroused strong interests. Through a combined quantum and molecular mechanics CASPT2/AMBER scheme taking terephthalic acid (TPA) as example, we found that electrostatic interaction not only can induce an enhanced radiative decay $T_1 \rightarrow S_0$ through the dipole-allowed S_1 intermediate state, but also can hinder the nonradiative decay process upon crystallization. From gas phase to crystal, the nature of S_1 state is converted to $^1(\pi,\pi^*)$ from $^1(n,\pi^*)$ character, enhancing transition dipole moment and serving as an efficient intermediate radiative pathway for $T_1 \rightarrow S_0$ transition, and eventually leading to a boosted RTP. The intermolecular packing also blocks the nonradiative decay channel of the high-frequency C═O stretching vibration with large vibronic coupling, rather than the conventional low-frequency aromatic rotation in crystal. This mechanism also holds for other organic compounds that contain both ketones and aromatic rings.

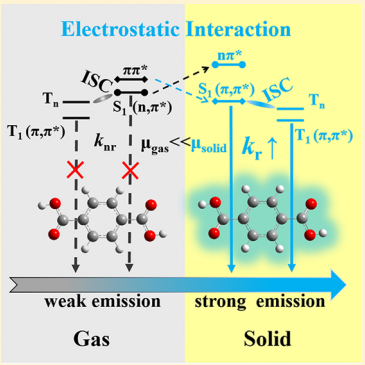

Very recently, room temperature phosphorescent (RTP) from pure organic materials[1−12] has attracted significant attention because, conventionally, RTP is extremely weak. Different mechanisms have been put forth to explain such exotic phenomena based on the discovered organic molecules in several experimental research groups. Adachi et al. showed that the carbazole derivatives embedded in β-estradiol as a host−guest material emit persistent RTP, which is highly deuterated to minimize the nonradiative deactivation.[4] Huang and co-workers claimed that the stabilized triplet states through H-aggregation intermolecular interaction is responsive for the long-lived RTP in a series of 1,3,5-triazines derivatives.[5] It is also reported that the carbazole-based ketones 4-(9Hcarbazol-9-yl)benzaldehyde (CZBA),[6] 4-(9H-carbazol-9-yl)-benzophenone (CZBP),[7] 4,4′-bis(9H-carbazol-9-yl)methanone (CZ2BP)[8] and phenothiazine-based dibenzothiophene-S,S-dioxide derivatives[9] showed boosted RTP, which were attributed to the enhanced intersystem crossing (ISC) from singlet to triplet states by ketones (C═O) and dibenzothiophene-S,S-dioxide (O═S═O) units and the suppressed nonradiative decay of triplet states through the restriction of intramolecular motion (RIM) upon crystallization, similar to the common aggregation-induced emission (AIE) systems.[10] Yang et al. and Xue et al. suggested that the intermolecular electronic coupling between benzophenone, dibenzothiophene-S,S-dioxide, heavy atom (bromine) and carbazole units can largely increase ISC from singlet to triplet states, leading to persistent RTP upon crystallization.[11,12] Interestingly, Tang and co-workers observed the crystallization-induced RTP in small aromatic acids[13] molecules, which was again attributed to RIM mechanism. It is highly intriguing to investigate the RTP from theoretical and computational perspective, which would gain deeper insight and eventually provide molecular design strategy.

In this Letter, we employed a combined quantum and molecular mechanics (QM/MM) approach, starting with terephthalic acid (TPA, see Chart 1) as example, to unravel the effect of crystallization on the nature of the molecular excited states. We found that from gas phase to crystal, the intermolecular electrostatic interaction not only converted state S_1 from $^1(n,\pi^*)$ to $^1(\pi,\pi^*)$, which increases the transition dipole moment and subsequently enhanced the radiative channel from T_1 to S_0, but also blocked the fast nonradiative decay process by the restriction of the high-frequency C═O stretching vibration rather than the conventional low-frequency aromatic rotational vibrations. The observed persistent RTP was thus attributed to such synergetic effect induced by the intermolecular electrostatic interaction on the decay of lowest triplet state T_1. We further demonstrate that this mechanism

Received: May 27, 2016
Accepted: July 14, 2016
Published: July 14, 2016

DOI: 10.1021/acs.jpclett.6b01156
J. Phys. Chem. Lett. 2016, 7, 2893−2898

Chart 1. Chemical Structure of (a) TPA and (b) QM/MM Models

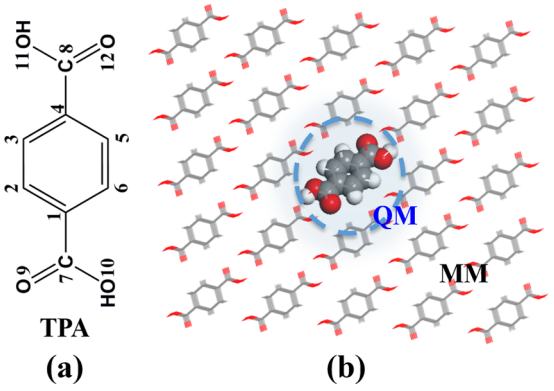

also works for other organic RTP compounds such as IPA[13] and CZ2BP.[8]

(A) Nature of the Lowest-Lying Excited States. To account for the fascinating crystallization-induced fluorescence and RTP for pure organic compounds, we calculate the excited-states structures for TPA molecule by using CASPT2 and hybrid CASPT2/AMBER with ANO-RCC-VDZP basis set in gas and solid phase, respectively, see Figure 1 and Table S1 for more

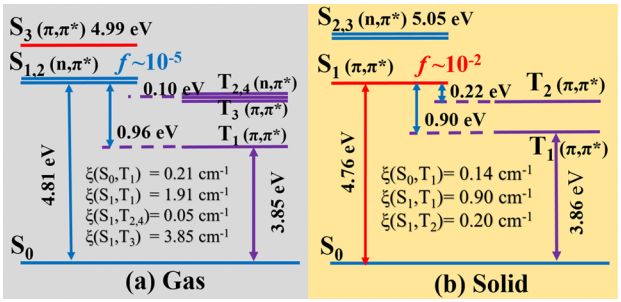

Figure 1. Calculated energy diagram, oscillator strengths (f) and spin−orbital coupling (ξ) of TPA in (a) gas phase and (b) solid phase by using CASPT2/ANO-RCC-VDZP at S_0-geometry.

detailed transition compositions, including the vertical excitation energies, nature of the states, oscillator strengths and spin−orbit couplings between low-lying singlet and triplet states. It is found that the nature of the lowest excited states S_1 becomes $^1(\pi,\pi^*)$ in solid from $^1(n,\pi^*)$ in gas phase, because the excitation energy of $^1(n,\pi^*)$ is raised up to 5.05 eV from 4.81 eV, whereas the $^1(\pi,\pi^*)$ state is reduced to 4.76 eV from 4.99 eV when going from gas to solid phases. Most importantly, the oscillator strength of S_1 is 3.33×10^{-5} in gas phase and is largely enhanced to 3.49×10^{-2} in crystalline phase. Namely, crystallization can induce the conversion from $^1(n,\pi^*)$ to $^1(\pi,\pi^*)$ for the S_1 state in TPA, which leads to fluorescence. It is also noted that in both gas phase and solid state, the T_1 is always of $^3(\pi,\pi^*)$. Thus, the transition energy $T_1 \rightarrow S_0$ and the spin−orbit coupling are almost unchanged, in sharp contrast to 3 orders of magnitude enhancement for the oscillator strength of $S_1 \rightarrow S_0$.

The enhanced phosphorescence in crystalline can be inferred from the electric transition dipole moment of $T_1 \rightarrow S_0$:[14]

$$\mu_{T_1 \rightarrow S_0} \propto \sum_n \frac{\xi(T_1, S_n)\mu_{S_n \rightarrow S_0}}{\Delta E_{T_1 \rightarrow S_n}} \quad (1)$$

where $\mu_{S_n \rightarrow S_0}$ is the electric transition dipole moment between the intermediate S_n singlet and ground states, $\xi(T_1,S_n)$ is the spin−orbit coupling (SOC) between the singlet S_n and lowest triplet T_1 states, and $\Delta E_{T_1 \rightarrow S_n}$ is the energy difference between T_1 and S_n. By keeping only $n = 1$ in the eq 1 for simplicity. Namely, the electrical transition dipole of $T_1 \rightarrow S_0$ consists of transition $T_1 \rightarrow S_1$ via spin−orbit coupling followed by spin and electric dipole-allowed $S_1 \rightarrow S_0$ transition. When going from gas to solid, the oscillator intensity of $T_1 \rightarrow S_0$ is increased to 4.24×10^{-10} from 9.30×10^{-12}. Thus, the crystallization induced RTP can be understood as the conversion of the S_1 from $^1(n,\pi^*)$ to $^1(\pi,\pi^*)$.

(B) Effect of the Intermolecular Electrostatic Interaction. To understand such a conversion, we look at the effects of intermolecular electrostatic interaction and molecular geometry modification: these are the two major crystallization effects at the molecular level. We examine the excited state structures for four different models in Figure 2a: the individual molecule

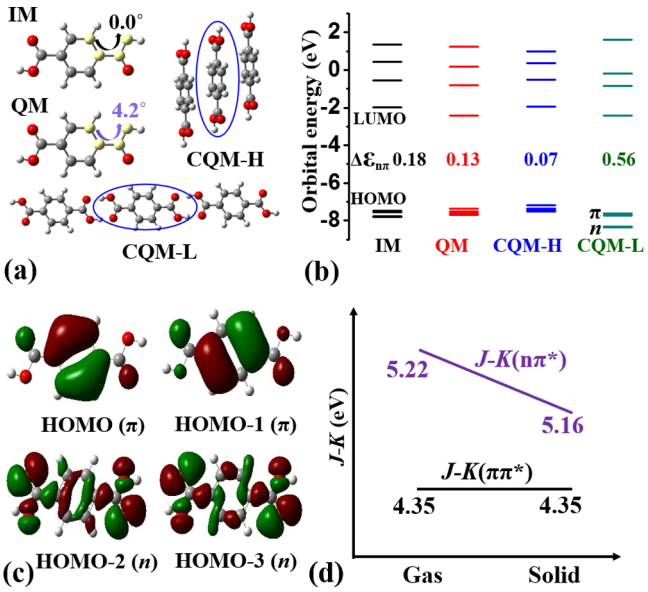

Figure 2. Diagram of (a) three models for TPA, (b) Kohn−Sham molecular orbital levels, (c) molecular orbitals, and (d) comparison of J-K for ($n\pi^*$) and ($\pi\pi^*$) transition. The IM, QM, CQM-H and CQM-L represent the isolated molecule, QM molecule in the cluster, and QM molecule surrounding background charge coming from MM molecules on the benzene ring side and the carboxyl group side in the cluster, respectively. $\Delta\varepsilon_{n\pi}$ represents the energy difference between HOMO−1 (π) and HOMO−2 (n).

(IM), the single molecule (QM) with molecular structure as embedded in the cluster, one molecule along with background charges coming from neighboring two molecules on its benzene ring side (CQM-H) and carboxyl group (−COOH) side (CQM-L) in the cluster, respectively. Namely, going from IM to QM, the difference stems from the molecular geometry. But from QM to CQM-H and CQM-L, the latter consist of a charged environment. Additionally, the influence of molecular packing on electronic transition characters were also inspected by comparing CQM-H with CQM-L. From the lowest three singlet excite states, it is found that the lowest excited state is of $^1(n,\pi^*)$ nature in IM, QM and CQM-H models but becomes $^1(\pi,\pi^*)$ for CQM-L. To save the computational cost dramatically, B3LYP/CC-PVDZ is used here owing to the

DOI: 10.1021/acs.jpclett.6b01156
J. Phys. Chem. Lett. 2016, 7, 2893−2898

similar excited-state properties presented in Table S2 with those of CASPT2 in Table S1. Table S3 summaries a comparison of these four situations for their lower excited states. This clearly shows that local electrostatic interaction surrounding carboxyl group (−COOH) plays a crucial role on the changed transition character of S_1 state from gas to solid. To gain a deeper insight on the electrostatic interaction, we have a look at the dipole and quadrupole moments of ground, low-lying states and environments for TPA molecule in Table S4 and S5 as well as those of the other compounds mentioned afterward. It is obvious that the transform between $^1(n,\pi^*)$ and $^1(\pi,\pi^*)$ states can be understood by the fact that the dipole moment of the $^1(\pi,\pi^*)$ state is larger than that of $^1(n,\pi^*)$ and ground states for a polar molecule,[15] while similar behavior is found for quadrupole moments in nonpolar molecules. This means the reverse of $^1(n,\pi^*)$ and $^1(\pi,\pi^*)$ states can be induced by enhanced electrostatic interaction, whether the molecule is polar or nonpolar. If we look at the frontier molecular orbitals (Figure 2b,c), one can find that the two degenerate n-orbitals (HOMO−2 and HOMO−3) are always lower than the degenerate π (HOMO and HOMO−1) ones. Band structure calculation performed for TPA crystal again confirmed that the two highest-lying valence bands are of π character, while the third and fourth bands are formed by lone-pair orbitals (see Figure S1). This demonstrates the reliability for our QM/MM approach, which is a practical way to handle the molecular excited state within solid environments.

To better understand such crossover for S_1 but not for T_1, we take a look at both the molecular orbitals and the Coulomb and exchange contributions to the excitation with the configuration interaction single (CIS) approximation. The singlet and triplet excited states are expressed as $E_S = \varepsilon_{ai} - (J - K)$ and $E_T = \varepsilon_{ai} - J$, respectively, where ε_{ai} is the energy difference between Hartree−Fock molecular orbitals a and i, J represents the Coulombic attraction ($-J$) between an electron at orbital a and a hole at orbital i, and K is the exchange energy. Within the frontier MOs, HOMO−2 is an n-orbital, HOMO and HOMO−1 are degenerate π-orbitals and LUMO is a π^*-orbital. At gas phase, the energy difference of highest occupied n and π orbitals ($\varepsilon_\pi - \varepsilon_n$) is 0.18 and 0.13 eV for IM and QM, respectively, and it is insensitive to the electrostatic interaction around the benzene ring due to the small energy difference (0.07 eV) in the CQM-H case. However, it is much more sensitive to the local electrostatic interaction surrounding the carboxyl group; namely, from QM to CQM-L, it goes from 0.13 to 0.56 eV. This is mainly because the n-orbital is largely stabilized by the electrostatic interaction, while π and π^* orbitals are insensitive to the electrostatic environments. In fact, the n-orbital represents negative charge in the oxygen attracting the positive charge in hydrogen of the neighboring molecule. This is the origin of the orbital stabilization. For the π and π^* orbitals, charge is delocalized, and, on average, there is no net charge in the orbitals. On the other hand, $(J - K)$ is larger for $^1(n,\pi^*)$ than for $^1(\pi,\pi^*)$ (see Figure 2d), and its relatively large change makes $^1(n,\pi^*)$ the lowest excited state for the gas phase but $^1(\pi,\pi^*)$ for the solid phase. Thus, a solid environment tends to destabilize $^1(n,\pi^*)$ excitation. However, for $^1(\pi,\pi^*)$, it is much less sensitive to the charged environment.

In order to get a closer look at such crossover behavior, we further build one more computational model with TPA molecule surrounded by two polar chloroforms (TCM) with separation d (see Figure 3a). TDDFT/B3LYP/CC-PVDZ is employed to calculate the excitation energy and the natural

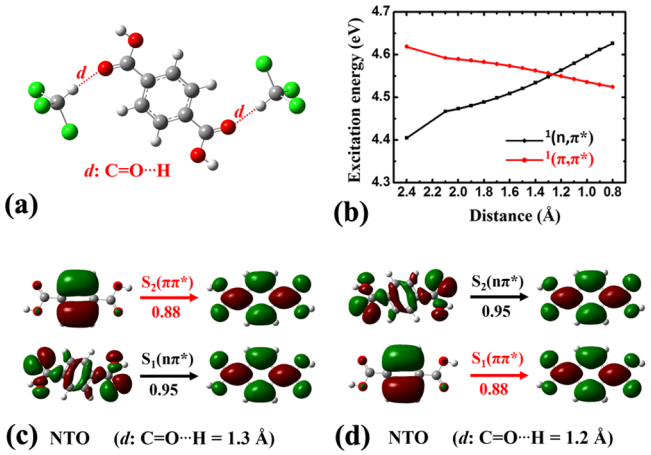

Figure 3. (a) TPA molecule surrounded by two polar chloroform molecules, (b) the excitation energy of the lowest $^1(n,\pi^*)$ and $^1(\pi,\pi^*)$ states as a function of intermolecular distance d (the charge distribution of chloroform was treated as background charges). The natural transition orbitals (NTOs) of the lowest $^1(n,\pi^*)$ and $^1(\pi,\pi^*)$ states at (c) C═O···H = 1.3 Å and (d) C═O···H = 1.2 Å are also depicted. It is noted that the TPA molecule is in the gas phase when d is 2.4 Å.

transition orbital (NTO) of the lowest-lying excited states S_1, S_2, and S_3 of TPA with the surrounding TCM modeled as a charge cloud extracted from ground state DFT calculation on the complex. It is found that (i) at a large separation, the lowest two excited states S_1 and S_2 are close to each other and both are of $^1(n,\pi^*)$ nature. S_3 is of $^1(\pi,\pi^*)$ excitation; (ii) with increasing electrostatic interaction by progressively moving the solvent TCM closer to TPA, it is found that the crossover of the $^1(n,\pi^*)$ and $^1(\pi,\pi^*)$ states occurs at a distance of ca. 1.3 Å between the H atom of TCM and the O atom of TPA (see Figure 3b).

This behavior is a well-established phenomenon in textbooks,[15] and has also been found in previous theoretical and experimental studies.[16−19] Using TDDFT combined with polarizable continuum model, it was shown that the lowest excited state of the uracil molecule is $^1(n,\pi^*)$ in the gas phase, but becomes the $^1(\pi,\pi^*)$ state when the solvent effect is considered.[16,17] Zhang et al. have shown that several aromatic ketone derivatives were weakly or even not fluorescent in CH_2Cl_2. As far as Lewis acids ($AlCl_3$, BCl_3, etc.) added in solution, strongly fluorescent emissions could be observed. These were claimed to be a conversion of the lowest excited state from $^1(n,\pi^*)$ to $^1(\pi,\pi^*)$ state with the aid of Lewis acid.[18] Kwon et al. have also reported that the 2,5-dihexyloxy-4-bromobenzaldehyde (Br6A) and its derivative G1 compounds showed weak fluorescence in low-polar solvents, but can emit strong fluorescence in strong polar solvents. They proposed that this phenomenon can be attributed to the lowest excited state transformation from $^1(n,\pi^*)$ to $^1(\pi,\pi^*)$ state with solvent polarity enhancing.[19]

(C) Singlet Excited State Decay: Radiative and Nonradiative Rates. The singlet excited state radiative decay and nonradiative decay are essential for light-emitting process. While the former can be simply estimated through Einstein spontaneous emission, the latter partly involves the energy dissipation through vibronic couplings, which can be characterized by the normal mode reorganization energy. We depict vibrational relaxation energy in the $S_1 \rightarrow S_0$ process for each mode in

DOI: 10.1021/acs.jpclett.6b01156
J. Phys. Chem. Lett. 2016, 7, 2893−2898

Figure 4. The reorganization energies in the low frequency region (less than 400 cm^{-1}) are almost zero both in gas and

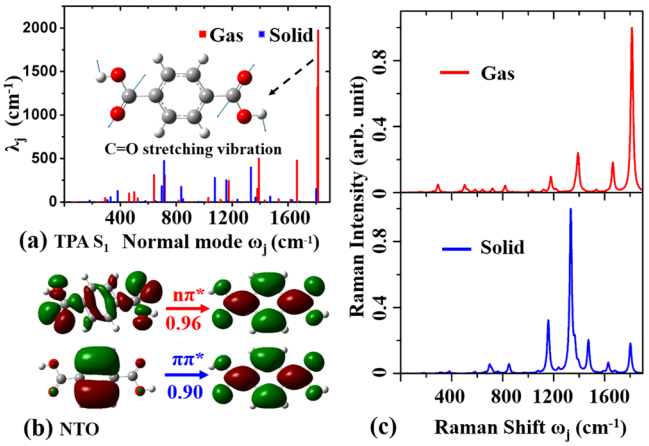

Figure 4. (a) Normal mode reorganization energy; (b) nature transition orbitals (NTOs) and (c) resonance Raman spectrum of TPA for the lowest singlet state both in gas and solid phases.

solid phases, excluding the contribution from the out-of-plane rotations of the aromatic rings. Interestingly, the C═O stretching vibration contributes the most (~1974.37 cm^{-1}) in gas phase, which is consistent with the corresponding large geometrical modification (0.08 Å between S_0 and S_1 states) in Table S6 and the lone-pair electron localized on the C═O bond (n→π^* transition) shown in Figure 4b. However, in the solid phase, this value is reduced to 212.96 cm^{-1}. Such a remarkable reduction is due to the alternation to $\pi \rightarrow \pi^*$ transition as shown in Figure 4b, which is decoupled with the C═O stretching vibration. This is further correlated to a tiny geometrical modification difference (0.01 Å) between S_0 and S_1 states as well as charge redistribution to benzene rings for $\pi \rightarrow \pi^*$ transition. In addition, from a geometrical point of view, the intermolecular hydrogen bond (see Figure S2) between O in the C═O bond and the hydrogen of the neighboring molecule could further suppress the relaxation of C═O bond. We thus conclude that the nonradiative decay process is blocked by the restriction of the high-frequency C═O stretching vibration, rather than the conventional low-frequency aromatic rotational vibration. The resonance Raman spectrum (RRS) were further simulated to confirm this point as shown in Figure 4c. From gas to solid, the high-frequency Raman intensity is hugely reduced. These evident differences not only show the restriction of the high-frequency C═O stretching vibration,[20] but also imply the transformation from $^1(n,\pi^*)$ to $^1(\pi,\pi^*)$ state for the lowest singlet excited state.

Now, from gas to solid, the internal conversion (k_{ic}) rate of $S_1 \rightarrow S_0$ is calculated by the home-built MOMAP program.[21] the k_{ic} of $S_1 \rightarrow S_0$ is decreased about 1 order of magnitude, from 4.97×10^7 s^{-1} to 5.15×10^6 s^{-1}, while the radiative decay rate (k_r) is largely enhanced by 3 orders of magnitude from 3.34×10^4 s^{-1} to 3.43×10^7 s^{-1}, primarily due to the enhanced oscillator strength of $\pi \rightarrow \pi^*$. This quantitatively explains the observed strong fluorescence as well as RTP in solid phase. The conventional RIM mechanism found in common AIE molecule is a secondary effect for RTP.

We are ready to illustrate the mechanism of the electrostatic interaction induced RTP in Figure 5. Namely, the electrostatic interaction activates an efficient radiative pathway from T_1 to S_0

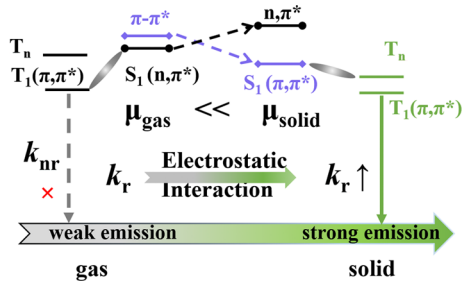

Figure 5. Proposed mechanism of electrostatic interaction induced long-lived RTP.

through converting S_1 from $^1(n,\pi^*)$ to $^1(\pi,\pi^*)$, inducing T_1 emission upon crystallization.

(D) Electrostatic Interaction-Induced RTP for IPA and CZ2BP. This proposed electrostatic interaction-induced phosphorescent mechanism is not only applicable for the TPA compound, but also valid for other compounds that contain both ketones and aromatic rings. The RTP has been recently demonstrated for isophthalic acid (IPA)[13] in crystal form and for 4,4′-bis(9H-carbazol-9-yl)methanone (CZ2BP) in cocrystal with chloroform.[8] We calculate the nature of the low-lying excited states by using (TD) B3LYP/CC-PVDZ for IPA, and (TD) CAM-B3LYP/CC-PVDZ for CZ2BP owing to its charge transfer character based on their optimized S_0-geoemtries both in gas and solid phases (see Figure 6). It is easily found that the S_1

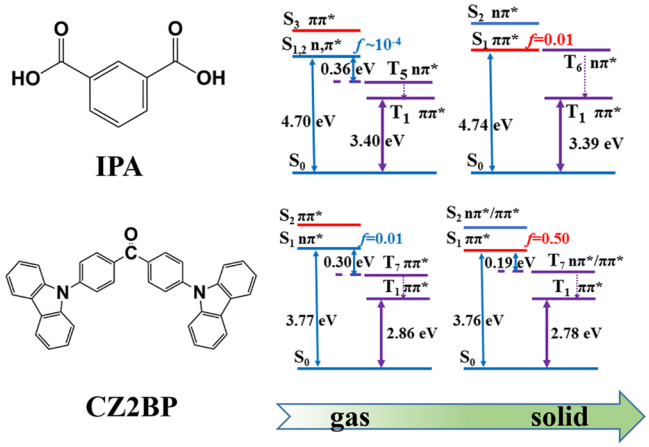

Figure 6. Illustration of the excited state structures and transition properties for IPA and CZ2BP.

states of these two compounds are inverted from $^1(n,\pi^*)$ to $^1(\pi,\pi^*)$ states from gas to crystalline phases and the oscillator strength of S_1 is significantly enhanced by 2 orders of magnitude: from 10^{-4} to 0.01 for IPA and from 0.01 to 0.50 for CZ2BP. Consequently, an efficient radiative decay pathway from T_1 to S_0 is expected through the intermediate states S_1. We also note that in solid phase, $S_1(\pi,\pi^*)$ is close in energy to T_6 or T_7. The latter is of $^1(n,\pi^*)$ character. Thus, according to the El-Sayed rule,[22] the intersystem crossing from S_1 to T_6 or T_7 is favored, in addition to the closeness in energy levels. These results independently support the proposed mechanism RTP of pure organic compounds.

In conclusion, we proposed a novel mechanism of electrostatic interaction induced phosphorescent mechanism and explain the recently discovered RTP from pure organic compounds in crystalline phase. Traditionally, this was regarded

DOI: 10.1021/acs.jpclett.6b01156
J. Phys. Chem. Lett. 2016, 7, 2893−2898

as rare. Through investigating the excited state electronic structures and radiative and nonradiative decay rates by a combined quantum mechanics and molecular mechanics (QM/MM) approach, we found that intermolecular electrostatic interaction can convert the lowest singlet excited state S_1 from $^1(n,\pi^*)$ type to $^1(\pi,\pi^*)$. This is primarily due to the destabilization of the lone-pair n-orbital within the charged environment. Band structure calculations on the nature of the frontier of valence bands further confirmed the reliability of the QM/MM model. Upon crystallization, the S_1 state is inverted as $^1(\pi,\pi^*)$ with a largely increased transition dipole moment by the introduced electrostatic interaction, and hence generates significantly enhanced radiative pathways $T_1 \rightarrow S_0$ through the intermediate state of S_1. Strikingly, the nonradiative decay process of S_1 is further suppressed in solid state through the restriction of the high-frequency C═O stretching vibration, rather than the common low-frequency intramolecular rotational vibration found in the conventional AIE systems. The proposed mechanism gives a clear description of the RTP behaviors for pure organic compounds TPA, IPA, and CZ2BP and is expected to be applicable for a class of organic molecules with lone pair n-orbitals.

METHODOLOGICAL APPROACH

The computational models were constructed by cutting a large cluster (5 × 5 × 5 supercell) from the crystal structure of TPA as shown in Chart 1. The quantum mechanics/molecular mechanics (QM/MM) method was implemented to deal with the electronic structures in crystal, where the central molecule is defined as the active QM part, and the surrounding ones are all rigid as the MM part. The atomic partial charges were generated by the restrained electrostatic potential (RESP)[23] method. The complete active space self-consistent field (CASSCF) and second-order perturbation (CASPT2) calculations were performed using MOLCAS[24] packages for the QM part, whereas AMBER-ff99 force field[25] was employed to deal with the MM part by using the Tinker[26] package. The interface between the QM and MM parts was coded by Ferré et al.[27] included in MOLCAS. The CASPT2//CASSCF method with the relativistic Atomic Natural Orbital basis set ANO-RCC-VDZP[28] was applied both in gas and solid phases. The 8 electrons in 8 orbitals (8*e*/8o) were chosen as active space (contour plot of the eight orbitals see Figure S3). These orbitals contain the two lone-pair *n* orbitals of carboxyl group and the π and π^* orbitals that are mainly distributed in the benzene ring. Vertical excitation energies, oscillator strengths, and spin−orbit coupling at the optimized structure (S_0) were determined from the 4-root state-averaged CASPT2//CASSCF calculations to include more dynamical electron correlations.

We further reoptimized the geometries and calculated the vibrational frequencies at S_0 and S_1 states at the (TD)B3LYP/CC-PVDZ level in order to determine the vibrationally coupled nonradiative decay rate of $S_1 \rightarrow S_0$. The gas-phase calculations were performed using Turbomole 6.5,[29] while the solid-phase ones were evaluated by using the same QM/MM model set up above by virtue of ChemShell 3.5,[30] interfacing Turbomole 6.5[29] for QM and DL_POLY[31] with the general Amber force field (GAFF)[32] for MM.

The radiative rate (k_r) is evaluated by the Einstein spontaneous emission relationship $k_r = \frac{fE_{vert}^2}{1.499 s \cdot cm^{-2}}$, where f is the dimensionless oscillator strength ($f = 2/3\ E_{vert}\mu^2$, μ is the transition dipole moment), and E_{vert} is the vertical excitation energy at the S_1-geometry. Especially, the electric transition dipole moment of $T_1 \rightarrow S_0$ can be obtained by eq 1. The reorganization energy and the nonradiative decay rate are calculated by our home-built package MOMAP program,[21] with detailed formulation in our recent review.[33] Excited state property analysis can be found in ref 34. Cartesian coordinates are used to construct the Duschinsky matrix and to calculate the reorganization energy.

ASSOCIATED CONTENT

Supporting Information

The Supporting Information is available free of charge on the ACS Publications website at DOI: 10.1021/acs.jpclett.6b01156.

The computational details and results for band structure of TPA; the frontier MOs, molecular packing arrangement in crystal, geometric, and electronic structures of ground- and excited-states in both gas and solid phases, and excitation information on IM, QM, and CQM models for TPA molecule; the dipole moments of ground, low-lying states and environments for TPA, IPA and CZ2BP molecules (PDF)

AUTHOR INFORMATION

Corresponding Authors

*Qian Peng. Tel: +86-10-82616830. E-mail: qpeng@iccas.ac.cn.

*Zhigang Shuai. Tel: +86-10-62797689. E-mail: zgshuai@tsinghua.edu.cn.

Notes

The authors declare no competing financial interest.

ACKNOWLEDGMENTS

This work is supported by the National Natural Science Foundation of China (Grant Nos. 21290191, 21503118, 21303213, 21473214, 91333202, and 91233105), the Ministry of Science and Technology of China through 973 program (Grant Nos. 2013CB834703 and 2015CB655002), and the Strategic Priority Research Program of the Chinese Academy of Sciences (Grant No. XDB12020200).

REFERENCES

(1) Hirata, S.; Totani, K.; Kaji, H.; Vacha, M.; Watanabe, T.; Adachi, C. Reversible Thermal Recording Media Using Time-Dependent Persistent Room Temperature Phosphorescence. *Adv. Opt. Mater.* **2013**, *1*, 438−442.

(2) Lehner, P.; Staudinger, C.; Borisov, S. M.; Klimant, I. Ultra-Sensitive Optical Oxygen Sensors for Characterization of Nearly Anoxic Systems. *Nat. Commun.* **2014**, *5*, 4460.

(3) Mukherjee, S.; Thilagar, P. Recent Advances in Purely Organic Phosphorescent Materials. *Chem. Commun.* **2015**, *51*, 10988−11003.

(4) Hirata, S.; Totani, K.; Zhang, J.; Yamashita, T.; Kaji, H.; Marder, S. R.; Watanabe, T.; Adachi, C. Efficient Persistent Room Temperature Phosphorescence in Organic Amorphous Materials under Ambient Conditions. *Adv. Funct. Mater.* **2013**, *23*, 3386−3397.

(5) An, Z.; Zheng, C.; Tao, Y.; Chen, R.; Shi, H.; Chen, T.; Wang, Z.; Li, H.; Deng, R.; Liu, X.; et al. Stabilizing Triplet Excited States for Ultralong Organic Phosphorescence. *Nat. Mater.* **2015**, *14*, 685−690.

(6) Xue, P.; Sun, J.; Chen, P.; Wang, P.; Yao, B.; Gong, P.; Zhang, Z.; Lu, R. Luminescence Switching of A Persistent Room-Temperature Phosphorescent Pure Organic Molecule in Response to External Stimuli. *Chem. Commun.* **2015**, *51*, 10381−10384.

(7) Gong, Y.; Chen, G.; Peng, Q.; Yuan, W. Z.; Xie, Y.; Li, S.; Zhang, Y.; Tang, B. Z. Achieving Persistent Room Temperature Phosphor-

DOI: 10.1021/acs.jpclett.6b01156
J. Phys. Chem. Lett. 2016, 7, 2893−2898

escence and Remarkable Mechanochromism from Pure Organic Luminogens. *Adv. Mater.* **2015**, *27*, 6195−6201.
(8) Li, C.; Tang, X.; Zhang, L.; Li, C.; Liu, Z.; Bo, Z.; Dong, Y. Q.; Tian, Y.-H.; Dong, Y.; Tang, B. Z. Reversible Luminescence Switching of an Organic Solid: Controllable On-Off Persistent Room Temperature Phosphorescence and Stimulated Multiple Fluorescence Conversion. *Adv. Opt. Mater.* **2015**, *3*, 1184−1190.
(9) Ward, J. S.; Nobuyasu, R. S.; Batsanov, A. S.; Data, P.; Monkman, A. P.; Dias, F. B.; Bryce, M. R. The Interplay of Thermally Activated Delayed Fluorescence (TADF) and Room Temperature Organic Phosphorescence in Sterically-Constrained Donor-Acceptor Charge-Transfer Molecules. *Chem. Commun.* **2016**, *52*, 2612−2615.
(10) Mei, J.; Leung, N. L. C.; Kwok, R. T. K.; Lam, J. W. Y.; Tang, B. Z. Aggregation-Induced Emission: Together We Shine, United We Soar! *Chem. Rev.* **2015**, *115*, 11718−11940.
(11) Xue, P.; Wang, P.; Chen, P.; Yao, B.; Gong, P.; Sun, J.; Zhang, Z.; Lu, R. Bright Persistent Luminescence from Pure Organic Molecules Through a Moderate Intermolecular Heavy Atom Effect. *Chemi. Sci.* **2016**, DOI: 10.1039/C5SC03739E.
(12) Yang, Z.; Mao, Z.; Zhang, X.; Ou, D.; Mu, Y.; Zhang, Y.; Zhao, C.; Liu, S.; Chi, Z.; Xu, J.; et al. Intermolecular Electronic Coupling of Organic Units for Efficient Persistent Room-Temperature Phosphorescence. *Angew. Chem., Int. Ed.* **2016**, *55*, 2181−2185.
(13) Gong, Y.; Zhao, L.; Peng, Q.; Fan, D.; Yuan, W. Z.; Zhang, Y.; Tang, B. Z. Crystallization-Induced Dual Emission from Metal- and Heavy Atom-Free Aromatic Acids and Esters. *Chemi. Sci.* **2015**, *6*, 4438−4444.
(14) Peng, Q.; Niu, Y.; Shi, Q.; Gao, X.; Shuai, Z. Correlation Function Formalism for Triplet Excited State Decay: Combined Spin-Orbit and Nonadiabatic Couplings. *J. Chem. Theory Comput.* **2013**, *9*, 1132−1143.
(15) Barltrop, J. A.; Coyle, J. D. *Principles of Photochemistry*; John Wiley & Sons Press: Chichester, New York, Brisbane, Toronto, 1978.
(16) Improta, R.; Barone, V. Absorption and Fluorescence Spectra of Uracil in the Gas Phase and in Aqueous Solution: a TD-DFT Quantum Mechanical Study. *J. Am. Chem. Soc.* **2004**, *126*, 14320−14321.
(17) Ren, H.-S.; Li, Y.-K.; Zhu, Q.; Zhu, J.; Li, X.-Y. Spectral Shifts of the n→π^* and π→π^* Transitions of Uracil Based on a Modified Form of Solvent Reorganization Energy. *Phys. Chem. Chem. Phys.* **2012**, *14*, 13284−13291.
(18) Zhang, X.; Xie, T.; Cui, M.; Yang, L.; Sun, X.; Jiang, J.; Zhang, G. General Design Strategy for Aromatic Ketone-Based Single-Component Dual-Emissive Materials. *ACS Appl. Mater. Interfaces* **2014**, *6*, 2279−2284.
(19) Kwon, M. S.; Jordahl, J. H.; Phillips, A. W.; Chung, K.; Lee, S.; Gierschner, J.; Lahann, J.; Kim, J. Multi-Luminescent Switching of Metal-Free Organic Phosphors for Luminometric Detection of Organic Solvents. *Chemi. Sci.* **2016**, *7*, 2359−2363.
(20) Zhang, T.; Ma, H. L.; Niu, Y. L.; Li, W. Q.; Wang, D.; Peng, Q.; Shuai, Z. G.; Liang, W. Z. Spectroscopic Signature of the Aggregation-Induced Emission Phenomena Caused by Restricted Nonradiative Decay: A Theoretical Proposal. *J. Phys. Chem. C* **2015**, *119*, 5040−5047.
(21) Shuai, Z. G.; Peng, Q.; Niu, Y. L.; Geng, H. MOMAP, A Free and Open-Source Molecular Materials Property Prediction Package; Revision 0.2.004; Available Online: http://www.shuaigroup.net/; Shuai Group: Beijing, 2014.
(22) El-Sayed, M. A. Triplet State. Its Radiative and Nonradiative Properties. *Acc. Chem. Res.* **1968**, *1*, 8−16.
(23) Bayly, C. I.; Cieplak, P.; Cornell, W.; Kollman, P. A. A Well-Behaved Electrostatic Potential Based Method Using Charge Restraints for Deriving Atomic Charges: The RESP Model. *J. Phys. Chem.* **1993**, *97*, 10269−10280.
(24) Aquilante, F.; De Vico, L.; Ferré, N.; Ghigo, G.; Malmqvist, P. å.; Neogrády, P.; Pedersen, T.; Pitoňák, M.; Reiher, M.; Roos, B. O.; et al. MOLCAS 7: The Next Generation. *J. Comput. Chem.* **2010**, *31*, 224−247.
(25) Moyna, G.; Williams, H. J.; Nachman, R. J.; Scott, A. I. Conformation in Solution and Dynamics of a Structurally Constrained Linear Insect Kinin Pentapeptide Analogue. *Biopolymers* **1999**, *49*, 403−413.
(26) Ponder, J. W.; Richards, F. M. An Efficient Newton-Like Method for Molecular Mechanics Energy Minimization of Large Molecules. *J. Comput. Chem.* **1987**, *8*, 1016−1024.
(27) Ferré, N.; Cembran, A.; Garavelli, M.; Olivucci, M. Complete-Active-Space Self-Sonsistent-Field/Amber Parameterization of the Lys296-retinal-Glu113 Rhodopsin chromophore-Counterion System. *Theor. Chem. Acc.* **2004**, *112*, 335−341.
(28) Roos, B. O.; Lindh, R.; Malmqvist, P.-Å.; Veryazov, V.; Widmark, P.-O. Main Group Atoms and Dimers Studied with a New Relativistic ANO Basis Set. *J. Phys. Chem. A* **2004**, *108*, 2851−2858.
(29) Ahlrichs, R.; Bär, M.; Häser, M.; Horn, H.; Kölmel, C. Electronic Structure Calculations on Workstation Computers: The Program System Turbomole. *Chem. Phys. Lett.* **1989**, *162*, 165−169.
(30) Sherwood, P.; de Vries, A. H.; Guest, M. F.; Schreckenbach, G.; Catlow, R. C. A.; French, S. A.; Sokol, A. A.; Bromley, S. T.; Thiel, W.; Turner, A. J.; et al. QUASI: A General Purpose Implementation of the QM/MM Approach and Its Application to Problems in Catalysis. *J. Mol. Struct.: THEOCHEM* **2003**, *632*, 1−28.
(31) Smith, W.; Forester, T. R. DL_POLY_2.0: A General-Purpose Parallel Molecular Dynamics Simulation Package. *J. Mol. Graphics* **1996**, *14*, 136−141.
(32) Wang, J.; Wolf, R. M.; Caldwell, J. W.; Kollman, P. A.; Case, D. A. Development and Testing of a General Amber Force Field. *J. Comput. Chem.* **2004**, *25*, 1157−1174.
(33) Shuai, Z.; Peng, Q. Organic Light-Emitting Diodes: Theoretical Undersdtanding of Highly Efficient Materials and Development of Computational Methodology. *Nat. Sci. Rev.* **2016**, DOI: 10.1093/nsr/nww024.
(34) Laurent, A. D.; Jacquemin, D. Analyzing Excited-state Processes and Optical Signatures of A Ratiomeric Fluorine Anion Sensor: A Quantum Look. *Sci. China: Chem.* **2014**, *57*, 1363−1368.

DOI: 10.1021/acs.jpclett.6b01156
J. Phys. Chem. Lett. 2016, 7, 2893−2898